Table S1. Statistics of cryo-EM data and atom model refinements

Dataset	aleniglipron-GLP-1R-Gs (EMDB-64939 / PDB: 9VC1)	lotiglipron-GLP-1R-Gs (EMDB-64940 / PDB: 9VC2)	compound 73-GLP-1R-Gs (EMDB-64941 / PDB: 9VC3)	compound 355-GLP-1R-Gs (EMDB-64942 / PDB: 9VC4)	compound 3b-GLP-1R-Gs (EMDB-64943/ PDB: 9VC5)
Data collection and processing					
Microscope	Titan Krios G3i	Titan Krios G3i	Titan Krios G3i	Titan Krios G4	Titan Krios G4
Magnification	130,000	130,000	130,000	96,000	96,000
Voltage (kV)	300	300	300	300	300
Electron exposure (e-/Å^2)	50	50	50	50	50
Defocus range (μm)	-0.8 to -1.8	-0.8 to -1.8	-0.8 to -1.8	-0.8 to -1.8	-0.8 to -1.8
Pixel size (Å) (calibrated)	0.932	0.932	0.932	0.81	0.81
Total exposure (e-/Å^2)	50	50	50	50	50
Symmetry imposed	C1	C1	C1	C1	C1
Initial particle images (no.)	6,924,935	4,766,036	7,514,542	4,458,347	5,240,200
Final particle images (no.)	657,890	1,157,699	1,390,623	256,525	425,839
Map resolution (Å, FCS 0.143)	2.5	2.3	2.4	3.0	3.0
Map resolution range (Å)	2.1 – 3.3	1.9 – 3.1	2.1 – 3.3	2.5 – 3.7	2.4 – 3.6
Refinement					
Initial model used (PDB code)	6X18	6X1A	6X18	6X1A	6X1A
Model resolution (Å, FCS 0.5)	2.6	2.4	2.6	3.2	3.1
Map sharpening B factor (Å^2)	98.4	93.9	103.1	158.4	163.0
Model composition					
Non-hydrogen atoms	3296	3270	3253	2630	2677
Protein residues	386	390	387	312	312
Ligands	1	1	1	1	3
B factors (Å^2)					
Protein	72.34	56.70	67.47	70.14	72.72
ligand	37.90	29.29	35.30	79.56	90.04
Validation					
MolProbity score	1.34	0.97	1.09	1.32	1.02
Clashscore	2.19	2.03	1.75	2.69	1.31
Poor rotamers (%)	0	0	0	0	0
RMSD from ideal values					
Bond length (Å)	0.003	0.002	0.002	0.004	0.003
Bond angle (°)	0.605	0.493	0.492	0.689	0.785
Ramachandran plot					
Favored/allowed/outlier (%)	95.00	98.19	97.11	96.10	97.08
Allowed	5.00	1.81	2.89	3.90	2.92
Disallowed	0	0	0	0	0

Figure S1. Cryo-EM data imaging and processing of aleniglipron-GLP-1R:Gs complexes. (a) Flowchart for EM data processing. (d) exemplar micrograph. (c) Local resolution-filtered EM maps (consensus and receptor/ECD focused refinements) displaying local resolution (Å) colored from highest resolution (dark blue) to lowest resolution (red). (d) Gold standard Fourier shell correlation (FSC) curves for the final consensus maps and map validation from half maps, showing the overall nominal resolution. (e) Particle orientation distributions in the final 3D reconstruction.

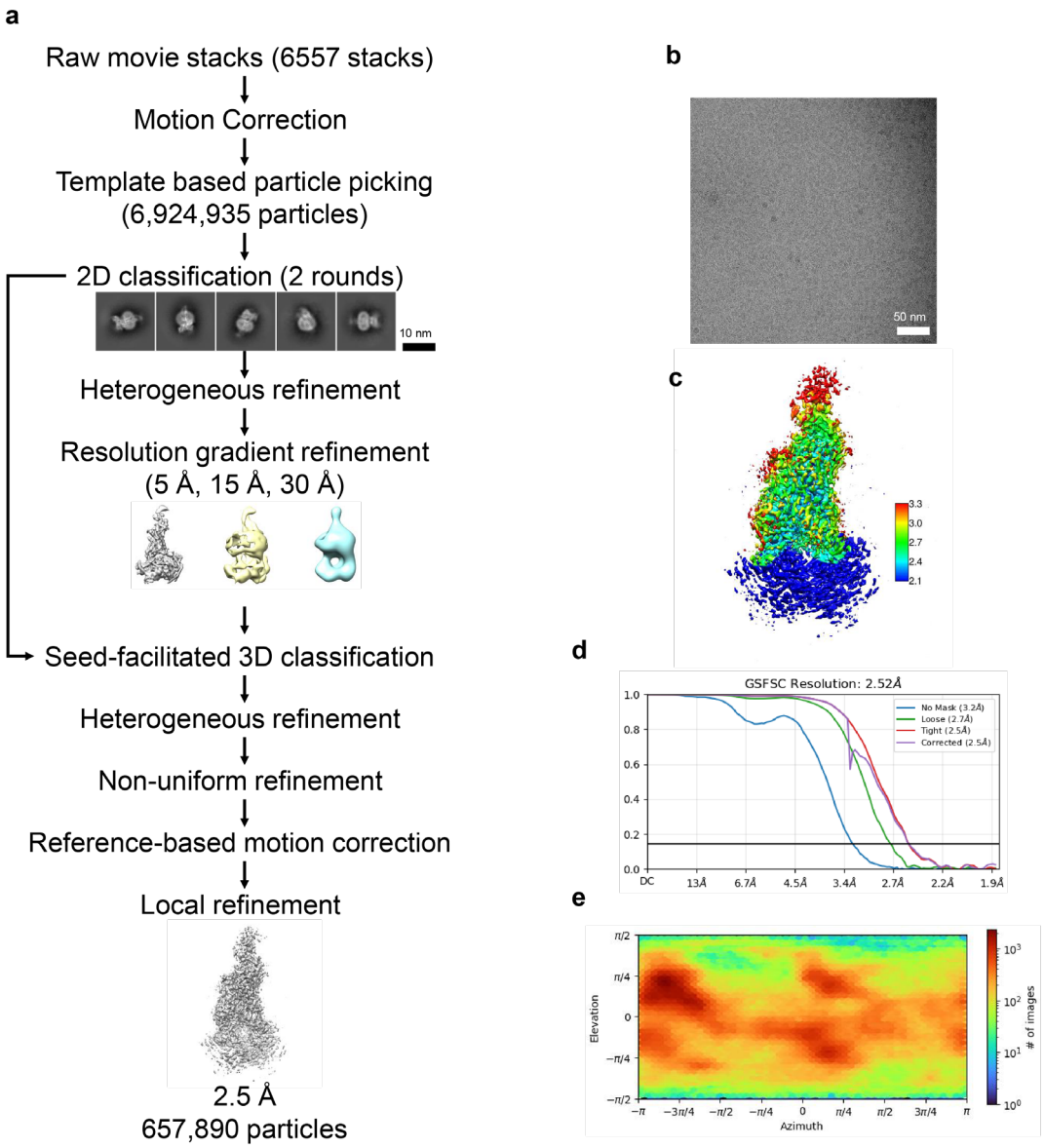

Figure S2. Cryo-EM data imaging and processing of lotiglipron-GLP-1R:Gs complexes. (a) Flowchart for EM data processing. (d) exemplar micrograph. (c) Local resolution-filtered EM maps (consensus and receptor/ECD focused refinements) displaying local resolution (Å) colored from highest resolution (dark blue) to lowest resolution (red). (d) Gold standard Fourier shell correlation (FSC) curves for the final consensus maps and map validation from half maps, showing the overall nominal resolution. (e) Particle orientation distributions in the final 3D reconstruction.

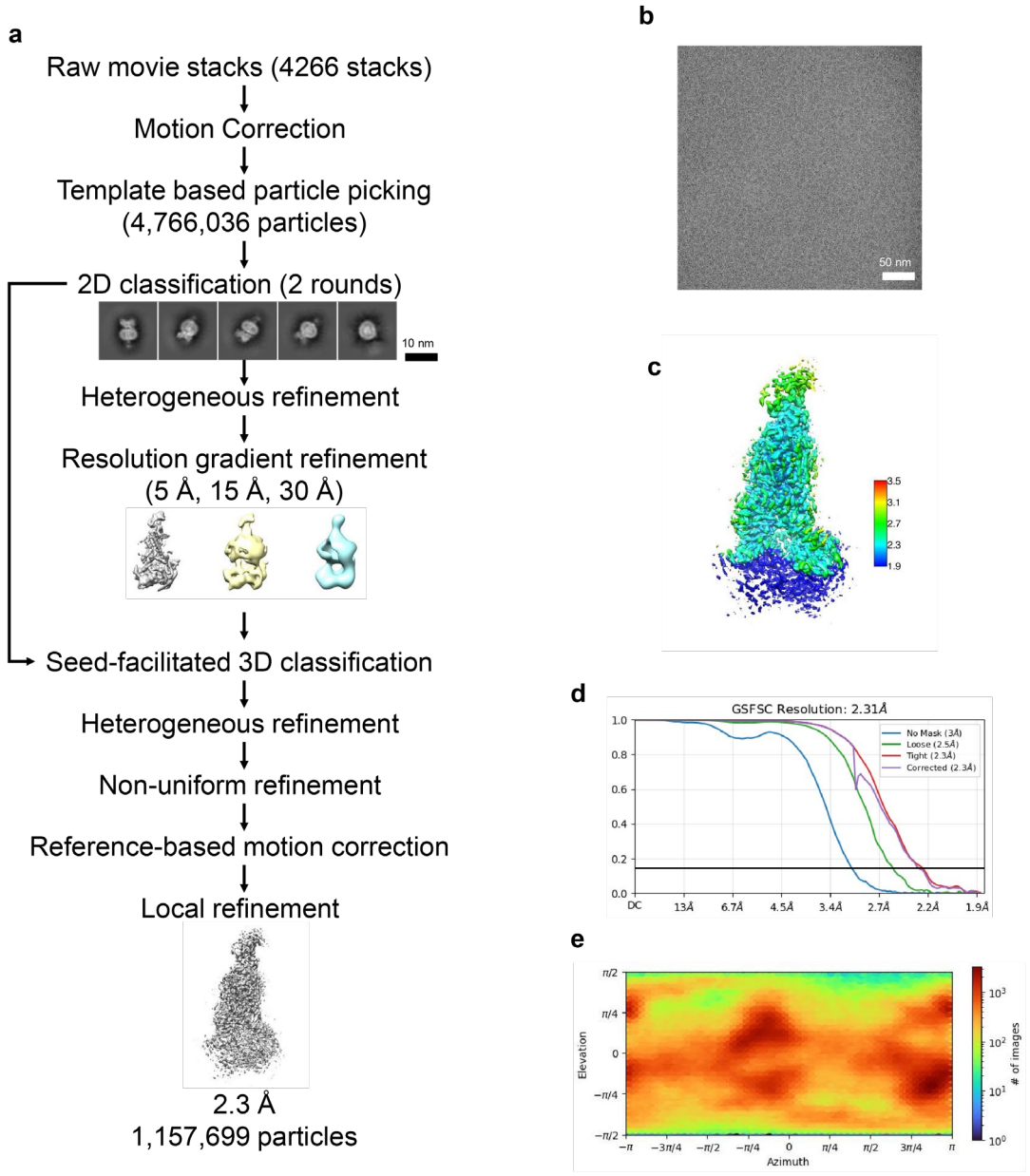

Figure S3. Cryo-EM data imaging and processing of compound 73-GLP-1R:Gs complexes. (a) Flowchart for EM data processing. (d) exemplar micrograph. (c) Local resolution-filtered EM maps (consensus and receptor/ECD focused refinements) displaying local resolution (Å) colored from highest resolution (dark blue) to lowest resolution (red). (d) Gold standard Fourier shell correlation (FSC) curves for the final consensus maps and map validation from half maps, showing the overall nominal resolution. (e) Particle orientation distributions in the final 3D reconstruction.

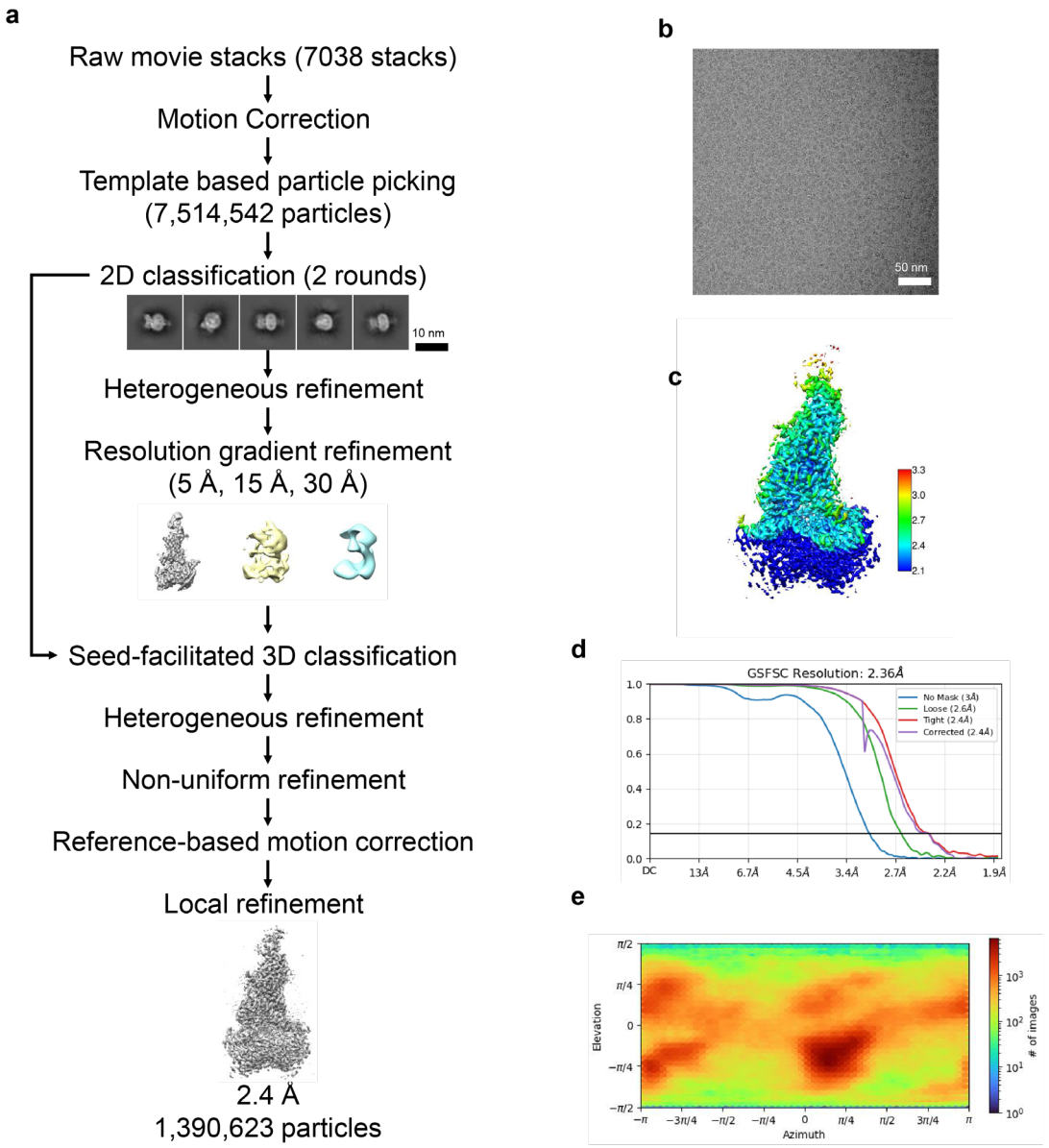

Figure S4. Cryo-EM data imaging and processing of compound 355-GLP-1R:Gs complexes. (a) Flowchart for EM data processing. (d) exemplar micrograph. (c) Local resolution-filtered EM maps (consensus and receptor/ECD focused refinements) displaying local resolution (Å) colored from highest resolution (dark blue) to lowest resolution (red). (d) Gold standard Fourier shell correlation (FSC) curves for the final consensus maps and map validation from half maps, showing the overall nominal resolution. (e) Particle orientation distributions in the final 3D reconstruction.

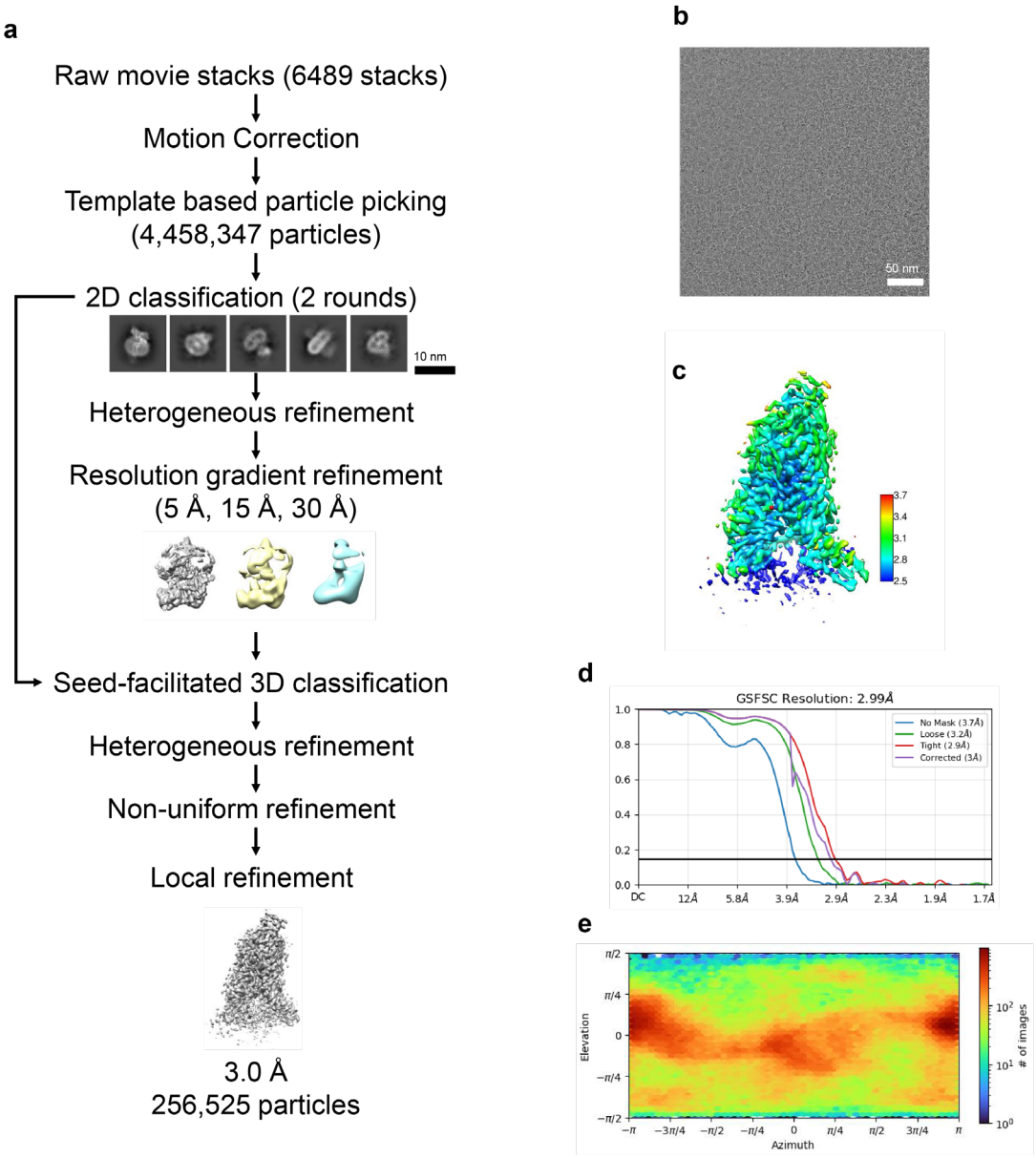

Figure S5. Cryo-EM data imaging and processing of compound 3b-GLP-1R:Gs complexes. (a) Flowchart for EM data processing. (d) exemplar micrograph. (c) Local resolution-filtered EM maps (consensus and receptor/ECD focused refinements) displaying local resolution (Å) colored from highest resolution (dark blue) to lowest resolution (red). (d) Gold standard Fourier shell correlation (FSC) curves for the final consensus maps and map validation from half maps, showing the overall nominal resolution. (e) Particle orientation distributions in the final 3D reconstruction.

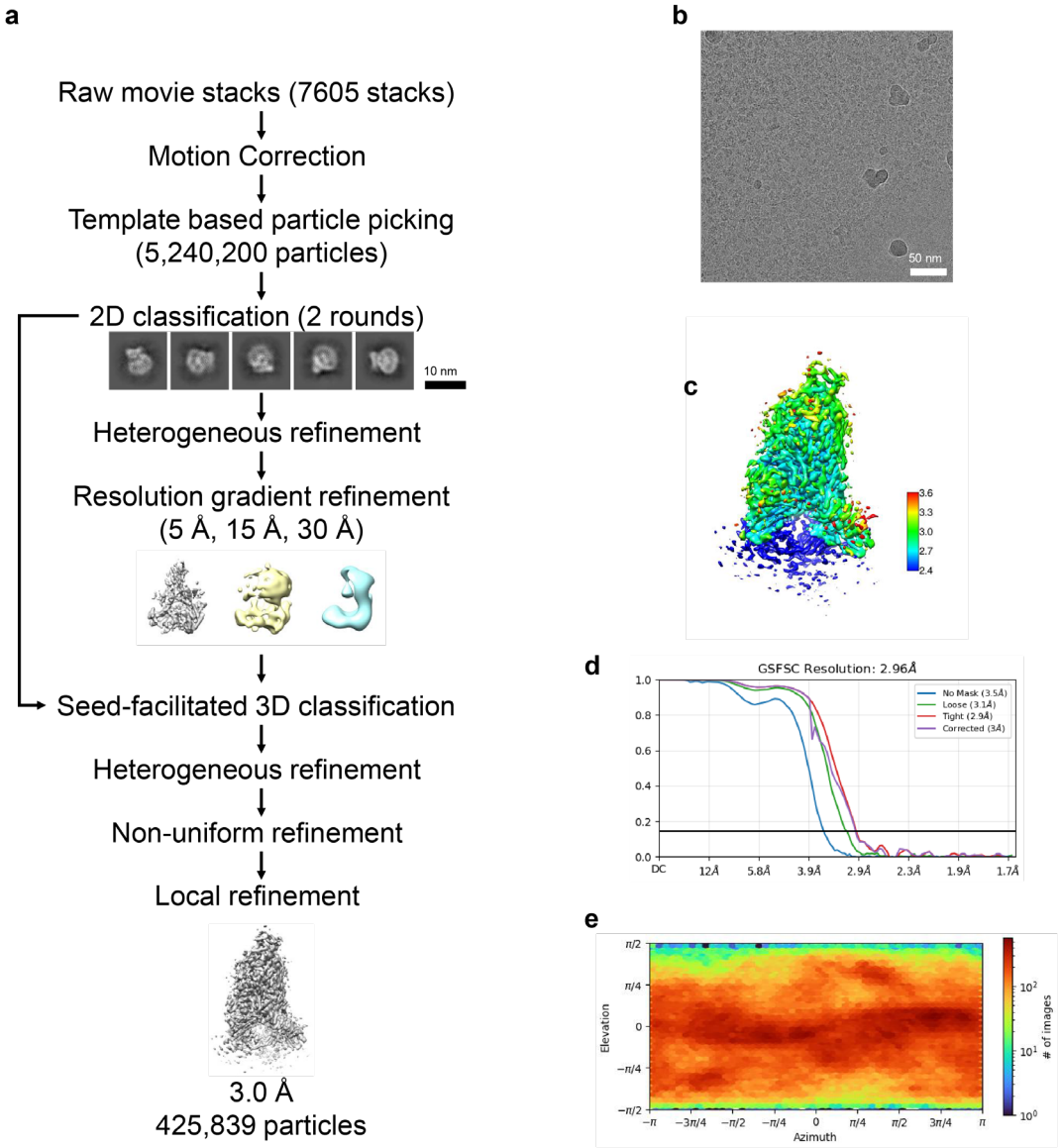

Figure S6. Atomic models of the ligands and receptors in the cryo-EM map. (a-e) EM density map and the model are shown for aleniglipron, lotiglipron, compound 73, compound 355, compound 3b, and all seven TM helices, and ECLs of the GLP-1R when bound to each agonist. All receptor and small molecules density was from the receptor-focused refined maps. ECL3 for compound 73 was poorly resolved and was not modelled.